

## Role of synthesis for oxygen defect incorporation in crystalline rubrene

Oleg Mitrofanov<sup>a)</sup>

Bell Labs, Alcatel-Lucent, Murray Hill, New Jersey 07974, USA and University College London, London WC1E7JE, United Kingdom

Christian Kloc

Bell Labs, Alcatel-Lucent, Murray Hill, New Jersey 07974, USA and Nanyang Technological University, Singapore 639798, Singapore

Theo Siegrist

Bell Labs, Alcatel-Lucent, Murray Hill, New Jersey 07974, USA

David V. Lang and Woo-Young So

Columbia University, New York, New York 10027, USA

Arthur P. Ramirez

Bell Labs, Alcatel-Lucent, Murray Hill, New Jersey 07974, USA and Columbia University, New York, New York 10027, USA

(Received 6 September 2007; accepted 31 October 2007; published online 20 November 2007)

Using photoluminescence characteristics at room temperature, we analyze incorporation of an oxygen-related defect, most likely rubrene peroxide, which produces an acceptor state in crystalline rubrene. Incorporation of rubrene-peroxide molecules can occur during the crystal growth as well as a result of the postgrowth oxidation, which depends on the presence of structural disorder. © 2007 American Institute of Physics. [DOI: 10.1063/1.2815939]

The growing understanding of the impact of molecular structure on charge transport and the versatility of the organic molecular synthesis provide great opportunities for control and manipulation of material properties. It is critical, however, to recognize that morphology and presence of defects, either structural or chemical, strongly affect the charge transport in organic solids. Single crystals are the optimal systems to investigate the impact of impurities and crystallographic defects. Crystals grown by the vapor transport sublimation method often exhibit a substantially higher purity and lower densities of crystallographic defects compared to crystals produced by solution-based methods or thin-film growth methods. The ability to control defect density in single crystals enables the determination of correlations between solid-state properties and the presence of defects and impurities.

Crystalline rubrene is the material of choice for studying the property/synthesis relationship. Rubrene crystals can exhibit hole mobilities in the range of 10–40 cm<sup>2</sup>/V s, the highest among the acenes and comparable to mobilities of amorphous silicon.<sup>1–3</sup> The observed large variation in electrical conductivity has led to a controversy about whether the conductivity increase is a result of impurity incorporation or an improvement in the crystal quality. Photoluminescence (PL) spectroscopy is an effective tool to address this issue since defects often produce characteristic spectral features. The PL analysis, however, relies on the knowledge of spectrum for the pure material. We showed recently that one of the commonly observed features in the spectrum of crystalline rubrene is caused by an oxygen-related impurity,<sup>4</sup> the presence of which also increases the conductivity.<sup>4–6</sup> In this letter, we provide further clarification of the optical spectra interpretation and analyze the impurity

incorporation processes using the spectral signature of the impurity.

Rubrene crystals are grown by the horizontal vapor transport method in a stream of argon gas.<sup>7</sup> To produce crystals with a low level of impurities, high-purity gas is used and the furnace is purged prior to growth. The growth process results in spontaneous formation of a large number of monocrystals with high-quality surfaces.<sup>8,9</sup> Rubrene samples with identified crystallographic axes are excited using the 442 nm line of a cw HeCd laser. The laser beam is focused using a 10× UV microscope objective to a spot with a diameter of about 100 μm. The laser spot position on the crystal surface is monitored using a magnifying imaging system. The average excitation intensity is 0.05 W/cm<sup>2</sup> unless specified otherwise. The laser excitation penetrates approximately 2 μm inside the samples. Room temperature PL emission is collected using the same microscope objective and projected on an input aperture of a spectrometer. The aperture spatially selects emission only from an area of the laser excitation with resolution better than 100 μm. The measured spectra represent the true surface-emitted PL characteristics and the waveguiding effects<sup>10</sup> are avoided.

Optical transitions in rubrene must be defined with respect to the molecular symmetry and orientation in the crystal. Rubrene crystallizes in an orthorhombic unit cell with space group symmetry (standard setting) *Cmca*  $D_{2h}^{18}$  (64) and lattice parameters  $a=26.901$  Å,  $b=7.187$  Å, and  $c=14.430$  Å.<sup>8,9</sup> Note that an alternative setting with transposed space group symbol *Bbcm* is often used. In this setting, the crystal axis directions are cyclically permuted from the standard setting ( $abc$ ) → ( $bca$ ) equivalent to a rotation of 120° about an axis in the  $\langle 111 \rangle$  direction of the Cartesian coordinate system.<sup>11</sup> In the *Bbcm* setting the lattice constants are  $a=7.187$  Å,  $b=14.430$  Å, and  $c=26.901$  Å. The  $c$ -axis direction is normal to the largest faces of the crystal and the  $b$  axis is normal to the long side faces (Fig. 1).<sup>8</sup> We will use

<sup>a)</sup>Electronic mail: o.mitrofanov@ucl.ac.uk

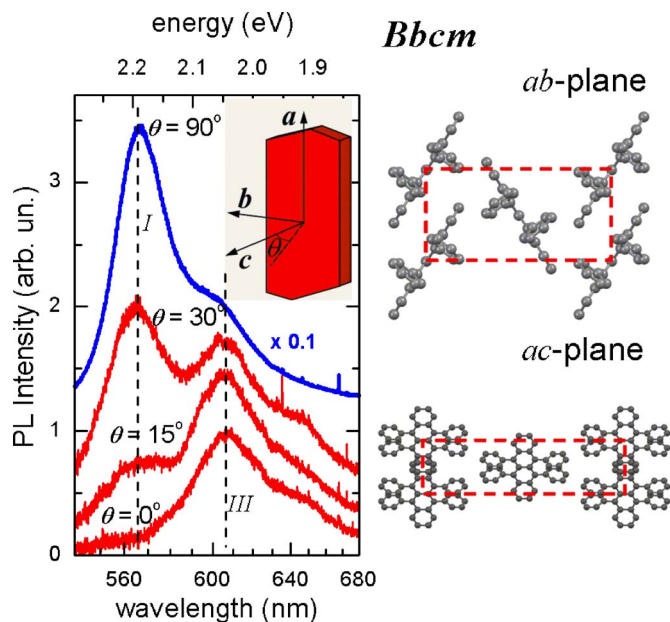


FIG. 1. (Color online)  $p$ -polarized spectra of a rubrene crystal measured at an angle  $\theta$  from the  $c$  axis. The  $\theta=90^\circ$  spectrum is measured on the  $ac$  surface with the incident laser polarization and the polarization analyzer oriented parallel to the  $c$  axis. Spectra are offset vertically for clarity. The crystallographic axes in the  $Bbcm$  setting are shown in the inset. The diagrams show the molecular packing on the  $ab$  and  $ac$  surfaces of the rubrene crystal.

the  $Bbcm$  setting throughout this work following other spectroscopic studies, for example Ref. 10. Two rubrene molecules in the unit cell form  $\pm 31.2^\circ$  angle between their long molecular axes  $L$  (along the tetracene backbone) and the crystal axis  $a$ . The  $L$  axes and the  $N$  axes (normal to the tetracene backbone plane) lie in the  $ab$  plane and the short molecular axes  $M$  are perpendicular to the  $ab$  plane.

A majority of rubrene studies are performed on the  $ab$  surface. A very weakly polarized PL band ( $III$ ) at 2.05 eV (605 nm) dominates in the spectra collected from this surface in our samples. Another band ( $I$ ) around 2.19 eV (567 nm) is often reported on the  $ab$  surface. This band exhibits a strong dependence on the angle from the normal  $\theta$ . There is very little or no emission in the direction normal to the  $ab$  surface (Fig. 1) and the band is  $p$ -polarized regardless of the emission direction. The dipole moment of the corresponding optical transition must be directed along the  $c$  axis. Because of this dipole moment orientation, the band dominates the emission spectra collected from the crystal side surfaces. Indeed, the 2.19 eV band is more than one order of magnitude stronger than the 2.05 eV band in spectra measured on the  $ac$  surface excited with the laser light polarized along the  $c$  axis. (Fig. 1). Note that the band maximum shifts to 2.16 eV if the excitation is polarized along the  $a$  axis.

It is important to realize that the emission polarized along the  $c$  axis appears in the spectrum collected from the  $ab$  surface only because the measurement is performed at an angle or the emission is collected within a nonzero solid angle. The same band polarized along the  $c$  axis was recently identified as due to emission from a crystal edge by Tavazzi et al.<sup>10</sup> Based on the polarization analysis of the PL data, we conclude that the 2.19 eV band corresponds to the  $M$ -polarized transition, and the 2.05 eV band to the  $L$ -polarized transitions. There is no splitting of the  $a$ - and  $b$ -polarized transition energies. It is consistent with the align-

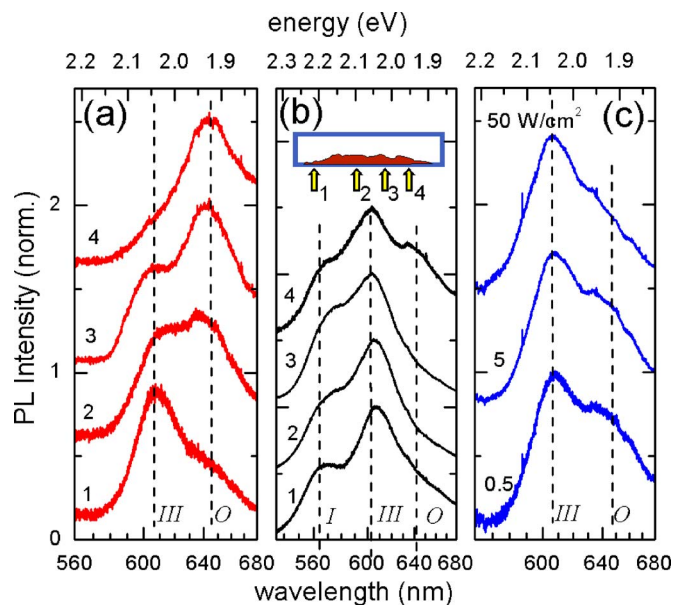


FIG. 2. (Color online) (a) Spectra of rubrene crystals grown in pure argon gas (1), unintentionally contaminated argon gas (2,3), and an argon/oxygen mixture (4). (b) Spectra of crystals sampled from a 50 mm long crystal growth zone. Samples 1–4 were grown at  $x=7, 20, 30,$  and  $40$  mm, respectively, where  $x$  is the position along the direction of the gas flow. The growth temperature is different for each sample:  $T_1 > T_2 > T_3 > T_4$ . (c) Normalized spectra of a rubrene crystal with the  $O$ -band measured using different excitation power: 0.5, 5, and  $50 \text{ W/cm}^2$ .

ment of the  $a$ - and  $b$ -polarized absorption bands.

In addition to the PL bands described above, we recently identified a PL band at 1.92 eV ( $O$ -band) that is likely to be associated with an oxygen-related impurity.<sup>4</sup> The  $O$ -band was observed in oxidized samples on the  $ab$  surface and we demonstrated (using the two-photon excitation) that the emission originates from the surface.<sup>4</sup>

To demonstrate the impurity presence we show examples of PL spectra of different rubrene crystals containing the  $O$ -band of various intensity [Figs. 2]. Analysis of the PL characteristics measured immediately after the crystal growth process shows that the impurity can be incorporated during the growth if oxygen is present in the gas flow. In Fig. 2(a), spectra 1 and 4 correspond to crystals grown in a stream of the ultrahigh purity argon gas ( $N_7$ ) and an argon and oxygen mixture (90/10), respectively. The spectra of crystals grown using the gas mixture exhibit a well-developed  $O$ -band, while the band is absent if pure argon is used. It is important to note that absence of the  $O$ -band is achieved after purging the growth chamber. Residual oxygen or leaks can result in contamination of rubrene crystals. The corresponding spectra show a weak  $O$ -band (spectra 2 and 3).

In order to evaluate the factors affecting the impurity incorporation during the growth, we monitored the PL characteristics inside the furnace immediately after the growth. We found that a stronger  $O$ -band emission is always observed in crystals at the cooler end of the growth zone [Fig. 2(b)]. Thus a nonuniform distribution of impurities is expected in crystals, most likely as a result of the temperature gradient within the growth zone.

It is important to note that the  $O$ -band emission saturates at high excitation intensities. The series of spectra in Fig. 2(c) shows a reduction of the  $O$ -band intensity relative to the main 2.05 eV band, which scales linearly as the excitation

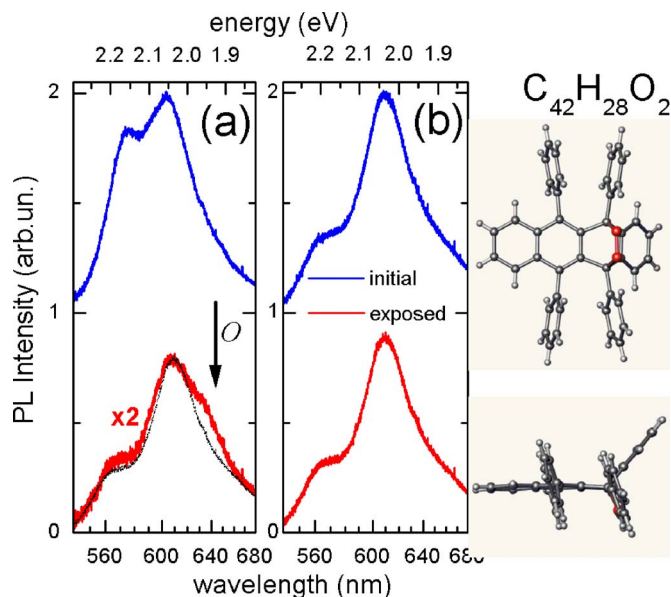


FIG. 3. (Color online) Effects of photo-oxidation on the PL spectrum for a commercially synthesized rubrene crystal with crystallographic defects (a) and for a high-quality vapor transport grown crystal (b). A small area (diameter of  $100\ \mu\text{m}$ ) in each sample is exposed to the laser beam ( $\lambda = 442\ \text{nm}$ ,  $P = 0.05\ \text{W}/\text{cm}^2$ ,  $b$ -polarized) for 7 h in air. The PL spectra are measured in the beginning and at the end of the exposure. The polarization analyzer is along the  $a$ -axis. The PL spectrum of the exposed crystal in panel (a) is multiplied by a factor of 2 for clarity. A thin black line in panel (a) shows a scaled spectrum of the exposed high-quality crystal from panel (b) for comparison.

power increases. We did not observe significant changes in the shape of the PL spectra for excitation powers below  $0.5\ \text{W}/\text{cm}^2$ . However, the saturation threshold is expected to vary with the impurity concentration.

These experimental facts confirm the conclusion of the earlier work<sup>4</sup> that emission of the  $O$ -band involves a defect-related electronic state, most likely due to rubrene peroxide. Indeed, rubrene peroxide molecules were recently detected on the surface of rubrene crystals by Kafer *et al.*<sup>12</sup> The impurity concentration gradually decreased with the depth indicating the surface oxidation mechanism. Another recent photo-oxidation study on amorphous rubrene films showed a bleaching effect typical for rubrene peroxide formation.<sup>13</sup> While the nature of the state is unclear at this point, it is likely that rubrene peroxide is the dominant oxygen-related impurity.

The present results allow further conclusions to be drawn about the oxidation process in rubrene crystals. The impurity incorporation can occur both during and after the growth. The degree of oxidation, determined by the relative intensity of the  $O$ -band, varies in rubrene crystals. Several crystals not exhibiting the  $O$ -band immediately after growth remained in the same state after one year in a normal ambient environment. Therefore, the presence of oxygen and light in the environment is not a sufficient condition to induce oxygen defects and another factor must be affecting the post-growth oxidation. We suggest that this factor is related to the presence of vacancies and dislocations in the crystal. The rubrene peroxide molecule has a significantly different configuration compared to the rubrene molecule, the backbone is bent by  $49.4^\circ$ , (Fig. 3). As a result, this molecule cannot be accommodated in a crystalline network of rubrene molecules. A vacancy, however, would provide the appropriate

steric relief allowing incorporation of the peroxide molecule.

In support of the hypothesis of defect-driven oxygen incorporation we compare the photo-oxidation process in a vapor transport grown crystal to that of a crystal selected from commercial rubrene powder. The latter is expected to contain a larger number of crystallographic defects and is presumably prone to oxidation. The evolution of the PL characteristics under laser exposure is drastically different for the two cases: while the PL yield decreases with time in the powder sample and a small shoulder appears in the region of the  $O$ -band [Fig. 3(a)], the vapor transport sample exhibits no change [Fig. 3(b)]. The robustness of the vapor transport grown crystals is encouraging for the development of rubrene-based devices. The crystal lattice possibly suppresses the rubrene-oxygen reaction.

A large number of experimental results presented here indicate that the rubrene peroxide impurity produces a band ( $O$ -band) in the PL spectrum of rubrene crystals. The  $O$ -band is sometimes mistakenly regarded as a spectroscopic signature of pure crystalline rubrene. The present work conclusively shows a direct causal relationship of the band presence with impurity incorporation. We also emphasize that there is a possible effect of structural disorder (in a form of vacancies, grain boundaries and dislocations) on rubrene's susceptibility to the oxidation process.

Finally, the effects of impurities on charge transport in rubrene crystals are yet to be fully understood. We recently concluded that the oxygen-related impurity produces a localized acceptor state within the bandgap.<sup>4-6</sup> There are, however, still open questions about the nature of the state and the mechanisms by which the state affects the carrier transport. Understanding of the origins of PL bands in rubrene and a thorough quantitative analysis of both the PL data and the transport data will allow making direct correlations between the material quality and the solid-state properties.

This work was partially supported by the U.S. Department of Energy (DE-FG02-04ER46118).

<sup>1</sup>V. Podzorov, E. Menard, A. Borissov, V. Kiryukhin, J. A. Rogers, and M. E. Gershenson, *Phys. Rev. Lett.* **93**, 086602 (2004).

<sup>2</sup>I. N. Hulea, S. Fratini, H. Xie, C. L. Mulder, N. N. Iossad, G. Rastelli, S. Ciuchi, and A. F. Morpurgo, *Nat. Mater.* **5**, 982 (2006).

<sup>3</sup>J. Takeya, M. Yamagishi, Y. Tominari, R. Hirahara, Y. Nikazawa, T. Nishikawa, T. Kawase, T. Shimoda, and S. Ogawa, *Appl. Phys. Lett.* **90**, 102120 (2007).

<sup>4</sup>O. Mitrofanov, D. V. Lang, C. Kloc, M. J. Wikberg, T. Siegrist, W.-Y. So, M. A. Sergent, and A. P. Ramirez, *Phys. Rev. Lett.* **97**, 166601 (2006).

<sup>5</sup>W.-Y. So, J. M. Wikberg, D. V. Lang, O. Mitrofanov, C. Kloc, T. Siegrist, M. A. Sergent, and A. P. Ramirez, *Solid State Commun.* **142**, 483 (2007).

<sup>6</sup>C. Krellner, S. Haas, C. Goldmann, K. P. Pernstich, D. J. Gundlach, and B. Batlogg, *Phys. Rev. B* **75**, 245115 (2007).

<sup>7</sup>R. A. Laudise, C. Kloc, P. G. Simpkins, and T. Siegrist, *J. Cryst. Growth* **187**, 449 (1998).

<sup>8</sup>B. D. Chapman, A. Checco, R. Pindak, T. Siegrist, and C. Kloc, *J. Cryst. Growth* **290**, 479 (2006).

<sup>9</sup>O. D. Jurchescu, A. Meetsma, and T. T. M. Palstra, *Acta Crystallogr., Sect. B: Struct. Sci.* **62**, 330 (2006).

<sup>10</sup>S. Tavazzi, A. Borghesi, A. Papagni, P. Spearman, L. Silvestri, A. Yassar, A. Camposeo, M. Polo, and D. Pisignano, *Phys. Rev. B* **75**, 245416 (2007).

<sup>11</sup>T. Hahn, *International Tables for Crystallography* (Reidel, Dordrecht, 1983), Vol. A, pp. 292–293.

<sup>12</sup>D. Kafer and G. Witte, *Phys. Chem. Chem. Phys.* **7**, 2850 (2005).

<sup>13</sup>M. Kytka, A. Gerlach, F. Schreiber, and J. Kovac, *Appl. Phys. Lett.* **90**, 131911 (2007).